1 **Search for hydrogen peroxide in the Martian atmosphere by the Planetary**

2 **Fourier Spectrometer onboard Mars Express**

3

4

5 Shohei Aoki [a,b,*], Marco Giuranna [b], Yasumasa Kasaba [a], Hiromu Nakagawa [a], Giuseppe

6 Sindoni [b], Anna Geminale [b], and Vittorio Formisano [b]

7

8 [a] Department of Geophysics, Graduate School of Science, Tohoku University, Sendai, Miyagi

9 980-8578, Japan

10 [b] Istituto di Astrofisica e Planetologia Spaziali (IAPS), Istituto Nazionale di Astrofisica

11 (INAF), Via del Fosso del Cavaliere 100, 00133 Roma, Italy

12

13

14

15

16

17

18

19

20

1   **Abstract**

2   We searched for hydrogen peroxide (H_2O_2) in the Martian atmosphere using data measured by

3   the Planetary Fourier Spectrometer (PFS) onboard Mars Express during five Martian years

4   (MY27–31). It is well known that H_2O_2 plays a key role in the oxidizing capacity of the

5   Martian atmosphere. However, only a few studies based on ground-based observations can be

6   found in the literature. Here, we performed the first analysis of H_2O_2 using long-term

7   measurements by a spacecraft-borne instrument. We used the v_4 band of H_2O_2 in the spectral

8   range between 359 cm^{-1} and 382 cm^{-1} where strong features of H_2O_2 are present around 362

9   cm^{-1} and 379 cm^{-1}. Since the features were expected to be very weak even at the strong band,

10   sensitive data calibrations were performed and a large number of spectra were selected and

11   averaged. We made three averaged spectra for different seasons over relatively low latitudes

12   (50°S–50°N). We found features of H_2O_2 at 379 cm^{-1}, whereas no clear features were detected

13   at 362 cm^{-1} due to large amounts of uncertainty in the data. The derived mixing ratios of H_2O_2

14   were close to the detection limits: 16 ± 19 ppb at $Ls = 0–120°$, 35 ± 32 ppb at $Ls = 120–240°$,

15   and 41 ± 28 ppb at $Ls = 240–360°$. The retrieved value showed the detection of H_2O_2 only for

16   the third seasonal period, and the values in the other periods provided the upper limits. These

17   long-term averaged abundances derived by the PFS generally agreed with the ones reported by

18   ground-based observations. From our derived mixing ratio of H_2O_2, the lifetime of CH_4 in the

19   Martian atmosphere is estimated to be several decades in the shortest case. Our results and

1   sporadic detections of CH_4 suggest the presence of strong CH_4 sinks not subject to

2   atmospheric oxidation.

3

1. Introduction

5   The atmosphere of Mars is strongly oxidized. Hydrogen radicals (H, OH, HO_2) play a key role

6   in regulating photochemistry in the Martian atmosphere, especially the oxidizing capacity.

7   Hydrogen peroxide (H_2O_2) represents a temporal reservoir of hydrogen radicals, and it is the

8   best tracer of oxidizers in the atmosphere because the abundance is relatively high. Presently,

9   only a few ground-based observations of H_2O_2 can be found in the literature (e.g., Encrenaz et

10 al., 2012). **Table 1** lists a summary of the H_2O_2 mixing ratios derived from these observations.

11 The observed values are distributed in the range from 0 to 50 ppb, and the maximum

12 abundance is observed during the northern autumn ($Ls = 206°$).

13   Understanding of oxidizing capacity in the Martian atmosphere is important to constrain

14 sinks of CH_4 on Mars. The spatial and temporal variation of CH_4 observed by ground-based

15 and space-borne instruments has led to much discussion on its sources and sinks (Formisano et

16 al., 2004; Mumma et al., 2009; Fonti and Marzo, 2010; Geminale et al., 2011). The

17 observations to date suggest that the lifetime of CH_4 in the Martian atmosphere is on the order

18 of weeks or months. In contrast, photochemical models have predicted that the photochemical

19 lifetime of CH_4 is 670 years (Wong et al., 2003), and the required loss rate of CH_4 is estimated

1 to be about 600 times faster than that predicted by the standard photochemical model (Lefèvre

2 and Forget, 2009). Since the main process that destroys CH_4 is oxidation by OH, long-term

3 averaged characteristics of H_2O_2 from Martian orbiters can provide further constraints on

4 oxidant loss of CH_4 in the Martian atmosphere.

5   The reason why H_2O_2 has not been detected by any instruments onboard Martian orbiters

6 is that the spectral resolutions were insufficient to distinguish the weak absorption lines of

7 H_2O_2 from the stronger ones of CO_2 and H_2O. The Planetary Fourier Spectrometer (PFS)

8 onboard Mars Express (MEX) has relatively high spectral resolution (~1.3 cm^{-1} without

9 apodization) in the spectral range between 250 and 8300 cm^{-1}. Mars Express has been

10 operating for ten years in Martian orbit since its launch in 2003, and the PFS has successfully

11 obtained a large amount of observational spectra. This dataset enables us to perform a

12 sensitive search for H_2O_2. Indeed, Encrenaz et al. (2012) pointed out that the PFS has the

13 potential to distinguish the weak absorption lines of H_2O_2 in the far-infrared range (350–400

14 cm^{-1}). In this paper, we attempted to perform detections of H_2O_2 from spacecraft-borne

15 measurements for the first time with the PFS data.

16

17 **2. Dataset and reduction**

18 The PFS is a Fourier transform spectrometer that was mainly designed for atmospheric

19 analyses such as measurements of the 3-D temperature field in the lower atmosphere,

1   variations of minor constituents, and optical properties of aerosols (Formisano et al., 2005). It

2   has two spectral channels: one is the Short Wavelength Channel (SWC) and the other is the

3   Long Wavelength Channel (LWC). The SWC covers the spectral range between 1750 and

4   8200 cm^{-1}, and the LWC covers the spectral range between 250 and 1700 cm^{-1}; both channels

5   have a sampling step of 1.0 cm^{-1}. The spectral resolution is 1.3 cm^{-1} without apodization and 2

6   cm^{-1} when a Hamming function is applied to the interferograms. One of the advantages of the

7   PFS is its wide spectral coverage with relatively high spectral resolution. An interferogram

8   can be obtained in about 4 s, with a repetition interval of 8.5 s. Its field of view is 1.6° for the

9   SWC and 2.8° for the LWC. In the period from January 2004 to August 2013, the PFS has

10   obtained about two million spectra of Mars. These cover almost all the regions of Mars for

11   different seasons and local times.

12   This study used the LWC data in the spectral range between 350 and 400 cm^{-1} (25.0–28.5

13   μm), which includes the strong absorption lines of H_2O_2 and H_2O. This spectral range does not

14   have strong lines of CO_2, and dust and water ice features are expected to be very weak in this

15   range (Smith et al., 2000). The previous observations have never used this spectral range for

16   studies of H_2O_2 because of the strong H_2O absorptions in the terrestrial atmosphere. **Figure 1**

17   shows the line strengths of H_2O_2 and H_2O obtained from the HITRAN08 database (Rothman

18   et al., 2009), and the synthetic spectra for the spectral resolution of the PFS (2.0 cm^{-1}) with

19   various mixing ratios of H_2O and H_2O_2 (details of the model are described in Section 3). As

1   pointed out in Encrenaz et al. (2012), the ν_4 band of H_2O_2 exhibits the strongest transition in

2   the considered spectral range and the PFS can detect H_2O_2 absorptions, although these are

3   very weak, at 362 and 379 cm^{-1}. In order to increase the signal to noise ratio (SNR), we

4   averaged thousands of spectra. The noise equivalent radiance (NER) of the PFS/LWC in the

5   considered spectral range (360–385 cm^{-1}) is around 1 erg/(s sr cm^2 cm^{-1}) (Giuranna et al.,

6   2005a). The measured radiance in this spectral range is typically ~90 erg/(s sr cm^2 cm^{-1}) at the

7   daytime low-latitude regions used in this study (i.e., SNR = 90 on a single spectrum). Thus,

8   the SNR reaches the order of 1000 by averaging thousands of spectra. In addition, we

9   performed sensitive calibrations in order to increase confidence in the tiny features of H_2O_2.

10   The PFS/LWC calibration has been presented in Giuranna et al. (2005a). Based on that, we

11   further improved the radiometric calibration. In-flight radiometric calibration uses the

12   measurements of an internal blackbody and deep space. The temperatures inside the

13   interferometer are very stable (Giuranna et al., 2005a), and they have remained stable during

14   the 10 years of PFS operations. We thus collected all the available calibration measurements

15   to derive the spectral responsivity and thermal emission of the instrument with a high degree

16   of confidence, and then we performed a re-calibration of the whole dataset using the new

17   accurate curves. Moreover, correction of asymmetric interferograms (phase correction) was

18   also improved. As shown in Giuranna et al. (2005a), the PFS produces ''double-sided''

19   interferograms; owing to phase errors, all original interferograms have an asymmetric form.

1 So far, the asymmetry of the central parts of the PFS interferograms were corrected by means

2 of a specially developed algorithm based on the method of phase correction suggested by

3 Forman et al. (1966). Recently, a new and improved algorithm has been developed and

4 applied to the PFS interferograms (Saggin et al., 2011). The implemented method is based on

5 the identification of an instrumental phase that is dependent on the interferometer temperature

6 and on the extraction of a linear phase component through a least-square approach. The use of

7 an instrumental phase parameterized with the interferometer temperature eases the

8 determination of the linear phase that can be extracted using only a narrow spectral region

9 selected to be immune from disturbances (Saggin et al., 2011). The procedure has been

10 intensively tested and successfully applied to whole datasets of the PFS. As a final remark, we

11 applied Hamming apodization to the interferograms used in this analysis. Although this

12 procedure slightly reduces spectral resolution, it significantly reduces side-lobes in the

13 instrumental line shape (Giuranna et al., 2005b).

14 In order to search for H_2O_2, we collected three averaged spectra for different seasonal

15 ranges: $Ls = 0–120°$, $Ls = 120–240°$, and $Ls = 240–360°$. We used the data collected during

16 the period from January 2004 to October 2011, which corresponds to five Martian years,

17 namely MY27 to MY31. Only nadir observations (emission angle less than 10°) were selected

18 for the analysis. In order to obtain a sufficient background radiance and reduce the uncertainty

19 due to averaging various atmospheric conditions, we built a reduced dataset where the latitude

1   is between -50° and +50°, local time is between 10 h and 16 h (dayside), and surface

2   temperature is between 250 K and 270 K. Finally, to further increase the homogeneity of

3   selected data, we only considered spectra acquired for fixed instrumental parameters such as

4   the spectral step, detector temperature, and position of the peak in the interferogram. In total,

5   the numbers of co-added spectra in the three averages are 20,260, 7477, and 13,777 for $Ls =$

6   0–120°, $Ls =$ 120–240°, and $Ls =$ 240–360°, respectively. In principle, the SNRs for the three

7   datasets reach to about 10,500, 6500, and 8600. **Figure 2** shows the distributions of solar

8   longitude L_s in the three datasets. Note that about 90% of the spectra in the first average were

9   acquired at $Ls =$ 0–60°, and about 80% of the spectra in the third average were acquired at Ls

10   = 330–360°.

11

12   **3. Method of analysis**

13   We retrieved the mixing ratio of H_2O_2 from comparisons between synthetic spectra and the

14   averaged PFS data in the spectral range between 359 and 382 cm^{-1}. For calculation of the

15   synthetic spectra, we developed a radiative transfer model for a plane-parallel and clear-sky

16   atmosphere by the line-by-line method. Radiance $I(v)$ is calculated by

17
$$I(v) = \varepsilon(v)B(T_{surf},v)e^{-\tau_n} + \sum_{i=1}^{n}\left(1 - e^{-(\tau_i - \tau_{i-1})}]B(T_{i-1/2},v)e^{-\tau_{i-1}}\right),$$

18   where v is the wavenumber, $\varepsilon(v)$ is the surface emissivity, and τ_i is the optical depth at the i-th

19   layer (Hanel et al., 2003). $B(T_{surf}, v)$ and $B(T_{i-1/2}, v)$ are the blackbody radiations at the Martian

1   surface temperature T_{surf} and the averaged temperature between the *i-th* and *i-1-th* atmospheric

2   layer, respectively. In this study, H_2O and H_2O_2 were considered as gaseous absorptions. The

3   surface emissivity $\varepsilon(v)$ was modeled as $\varepsilon(v) = \alpha v + \beta$, where α and β were constant parameters

4   (Smith et al., 2000; Fouchet et al., 2007). The spectroscopic parameters of the H_2O_2 lines were

5   obtained from the HITRAN08 database (Rothman et al., 2009), and those of H_2O lines were

6   obtained   from   the   water   vapor   line   list   for   a CO_2-rich   atmosphere

7   (http://astrobiology.gsfc.nasa.gov/Villanueva/spec.html). This database has the line shape

8   parameters (e.g., air-broadening coefficients) that were calculated for a CO_2-rich atmosphere

9   following the complex Robert Bonamy formalism based on the HITRAN08 database

10   (Villanueva et al., 2012). The terrestrial air-broadening coefficients of H_2O_2 are multiplied by

11   a factor of 1.5 uniformly in order to correct these values for the CO_2-rich atmosphere of Mars.

12   Temperature correction of the line intensity and temperature/pressure correction of the line

13   half-width were performed according to Rothman et al. (1998). The ratio of the total internal

14   partition function, which is required for the corrections mentioned above, was calculated using

15   the *"TIPS"* routine provided in the HITRAN08 database. The line shape function is assumed

16   to be the Voigt function (Drayson, 1976). The vertical profiles of temperature, pressure, and

17   H_2O were   obtained   from   the   Mars   Climate   Database   (MCD)   version   4.3

18   (http://www-mars.lmd.jussieu.fr). We   extracted   the   profiles   for   individual   observed

19   geometries and averaged them. The vertical profile of the H_2O_2 mixing ratio was assumed to

1   be uniform from 0 to 20 km (Encrenaz et al., 2012). The surface temperature was determined

2   from the averaged PFS spectrum between 300 and 500 cm^{-1}.

3   The synthetic spectrum to be compared with the PFS spectrum was obtained by a

4   convolution between the radiance $I(v)$ and the Instrumental Line Shape (ILS) of the PFS. The

5   ILS was obtained from the calibration measurements in the laboratory (Giuranna et al., 2005b).

6   As shown in Figure 9 of Giuranna et al. (2005b), the ILS has a weak side-lobe around -3 cm^{-1},

7   and its amplitude has a certain uncertainty. Since the effect of the side-lobe cannot be

8   neglected during comparisons to the absorption depth of H_2O_2, we set the amplitude as a

9   variable parameter in the retrieval process. In addition, we also set the spectral grid of the ILS

10   (i.e., spectral resolution) as a variable parameter because the peak position of the

11   interferogram varies slightly for different data, i.e., the spectral resolution should be slightly

12   modified.

13   In the retrieval process, we derived eight parameters: surface emissivity (α and β), the

14   scaling factor for the side-lobe of the ILS, the scaling factor for the spectral grid of the ILS,

15   the scaling factor for spectral grid of PFS, the scaling factor for the temperature profile, and

16   the mixing ratios of H_2O and H_2O_2. The scaling factor for the spectral grid of the PFS was

17   introduced because it is slightly shifted due to small temporal variations of the laser diode

18   temperature (Sindoni et al., 2011). The scaling factor for the temperature profile was

19   introduced because the water vapor lines are saturated and sensitive to the temperature profile.

1   Our retrieval was performed as follows: we prepared a parameter domain for the mixing ratio

2   of H_2O_2 from 0 to 100 ppb with intervals of 1 ppb. Then, we retrieved the other seven

3   parameters using the Levenberg–Marquardt non-linear minimization algorithm. Finally, we

4   derived the mixing ratio of H_2O_2 that provides the minimum values of the cost function χ^2.

5   The cost function χ^2 is defined as

6
$$\chi^2 = \frac{1}{N-M} \sum_{i=1}^{N} (\frac{y(v_i) - I(v_i)}{\sigma(v_i)})^2 \, ,$$

7   where v_i is i-th spectral point, N is the number of spectral points in the considered range (i.e.,

8    $N = 23$), M is the number of parameters (i.e., $M = 7$), $\sigma(v_i)$ is the noise of the averaged PFS

9   spectra, $y(v_i)$ is the averaged PFS spectrum, and $I(v_i)$ is the synthetic spectrum.

10

11   **4. Results and discussion**

12   **Figure 3** shows the averaged PFS spectra for the three different seasons. In the upper panels

13   of the figure, the averaged PFS spectra are compared to the synthetic spectra. The synthetic

14   spectra successfully reproduce the features of water vapor around 370 cm^{-1} and 375 cm^{-1}. The

15   best-fit synthetic spectra show that the column densities of water vapor are 2.43×10^{19} cm^{-2} at

16   $Ls = 0$–120°, 3.52×10^{19} cm^{-2} at $Ls = 120$–240°, and 2.50×10^{19} cm^{-2} at $Ls = 240$–360°, which

17   correspond to 7.25 pr-μm, 10.51 pr-μm, and 7.46 pr-μm, respectively. The absolute values and

18   the enhancement during the summer–autumn season are consistent with the previous reports

19   by spacecraft-borne observations (e.g., Smith, 2002). In the bottom panels of **Figure 3**, we

1   show residual spectra, where special synthetic spectra with all contributions except H_2O_2 have

2   been subtracted from the measured and synthetic spectra. The best-fit synthetic spectra show

3   that the mixing ratios of H_2O_2 are 16 ppb at $Ls = 0–120°$, 35 ppb at $Ls = 120–240°$, and 41 ppb

4   at $Ls = 240–360°$. As shown in the figures, H_2O_2 band-like features are clearly visible around

5   379 cm^{-1}. However, they were not detected around 362 cm^{-1}.

6   The black vertical bars shown in **Figure 3** represent the errors estimated from the noise

7   equivalent radiance divided by the square root of the number of measurements. However,

8   discrepancies between the synthetic spectra and the measured ones imply that the error bars

9   were underestimated. We think that this underestimation is due to the average of a number of

10 spectra that were taken under a wide range of different conditions (i.e., temperatures, water

11 vapor abundances, etc.). In order to evaluate realistic instrumental noises, we calculated the

12 standard deviation (1-sigma) of the residuals between the PFS data and best-fit synthetic

13 spectra. The red vertical bars shown in **Figure 3** represent the standard deviation. The SNRs

14 based on the standard deviation were about 3770 for the dataset averaged over $Ls = 0–120°$,

15 2630 for $Ls = 120–240°$, and 4330 for $Ls = 240–360°$. The uncertainties in the retrieved H_2O_2

16 mixing ratio owing to the instrumental noise (σ_n) were derived by comparisons between the

17 absorption depths of H_2O_2 and the retrieved standard deviation. The values are $\sigma_n = 19$ ppb at

18 $Ls = 0–120°$, $\sigma_n = 31$ ppb at $Ls = 120–240°$, and $\sigma_n = 27$ ppb at $Ls = 240–360°$. In addition to

19 the instrumental noise, uncertainties in the synthetic spectrum are the other sources of errors.

1   The dominant one among them is uncertainty in the line strength of H_2O_2 provided by the

2   HITRAN08 database, which is 10% at maximum (Rothman et al., 2009). The other sources of

3   model errors are due to the use of averaged temperatures, pressures, and water vapor, and due

4   to the effect of dust and water ice. The uncertainty due to the use of the "averaged

5   atmosphere" is estimated to be small and amounts to less than 1 ppb in the retrieved mixing

6   ratio of H_2O_2. The uncertainty due to the aerosols is also estimated to be small and amounts to

7   less than 5 ppb in the retrieved mixing ratio of H_2O_2. Finally, the error value in the retrieved

8   H_2O_2 mixing ratio σ was given by

9 $$\sigma = \sqrt{\sigma_n{}^2 + \sigma_{Int}{}^2 + \sigma_{avr}{}^2 + \sigma_{aer}{}^2},$$

10   where σ_n is error due to instrumental noise, σ_{Int} is that due to uncertainty in the line strength,

11   σ_{avr} is that due to using the "averaged atmosphere," and σ_{aer} is that due to ignoring the effect

12   of aerosols. The derived mixing ratios of H_2O_2 are 16 ± 19 ppb at Ls = 0–120° (i.e., 35 ppb

13   upper limit), 35 ± 32 ppb at Ls = 120–240°, and 41 ± 28 ppb at Ls = 240–360°.

14   The derived mixing ratios of H_2O_2 were close to the detection limits or upper limit because

15   of the large uncertainty owing to instrumental noise. However, the values generally agreed

16   with the ones reported by ground-based observations (see **Table 1**). Moreover, although the

17   error values are large, our results imply that the mixing ratio of H_2O_2 at Ls = 0–120° is

18   relatively low. The previous observations found similar aspects: IRTF/TEXES observations

19   showed that the mean mixing ratio is 10 ± 5 ppb at Ls = 80° and the upper limit is 10 ppb at Ls

1 $= 112°$ (Encrenaz et al., 2012), and Herschel/HIFI observations revealed the upper limit is 2

2 ppb at $Ls = 77°$ (Hartogh et al., 2010).

3 From the retrieved mixing ratio of H_2O_2, we can restrict the oxidizing capacity in the

4 Martian atmosphere and constrain the CH_4 sink on Mars. We calculated the CH_4 lifetime near

5 the surface assuming photochemical steady state. First, the HO_2 number density was estimated

6 from the observed H_2O_2 density:

7
$$[HO_2] = \sqrt{\frac{k_2[H_2O_2]}{k_1}} \, ,$$

8 where $[HO_2]$ and $[H_2O_2]$ represent the number densities, and k_1 and k_2 are the rate coefficients

9 of photochemical reactions shown in **Table 2.** Then, the OH number density was estimated

10 from the calculated HO_2 density, the observed H_2O_2 density, and the assumed densities of H_2O,

11 O_3, H, $O(^1D)$, H_2, and CO listed in **Table 3**:

12
$$[OH] = \frac{k_3[H_2O] + k_4[O_3][H] + k_5[HO_2][O] + 2k_6[H][HO_2] + 2k_2[H_2O_2] + k_7[HO_2] + 2k_8[O(^1D)][H_2O] + k_9[O(^1D)][H_2] + k_{10}[HO_2][O_3]}{k_{11}[O] + k_{12}[O_3] + k_{13}[HO_2] + k_{14}[H_2] + k_{15}[H_2O_2] + k_{16}[CO]} ,$$

13 where k_i is the rate coefficient of photochemical reactions shown in **Table 2.** In this equation,

14 the dominant terms are $2k_6[HO_2][O]$, $2k_2[H_2O_2]$, and $k_{16}[CO]$. This means that the OH

15 amount depends on those of HO_2 (which can be estimated from the H_2O_2 amount), H_2O_2, and

16 CO. **Figure 4a** shows the OH number density estimated from the H_2O_2 density. Finally, we

17 calculated the lifetime of CH_4 as follows:

18
$$\tau_{CH4} = \frac{1}{k_{17}[OH] + k_{18}[O(^1D)] + k_{19}[O]} ,$$

19 where k_{17}, k_{18}, and k_{19} are the rate coefficients of photochemical reactions shown in **Table 4**.

1   In this equation, $k_{17}[OH]$ is the dominant term.

2   **Figure 4b** shows the calculated lifetime of CH_4 associated with different H_2O_2 number

3   densities. Our observations showed that the averaged mixing ratio of H_2O_2 is between 0 and

4   70 ppb. The maximum value, i.e. 70 ppb, corresponds to 1.1×10^{10} cm^{-3} near the surface. The

5   calculated lifetime of CH_4 with this H_2O_2 abundance is about 50 years (solid line shown in

6   **Figure 4b)**, which is much longer than the observed lifetime on the order of weeks or months.

7   The short observed lifetime of CH_4 requires unrealistic large amounts of H_2O_2 that correspond

8   to 10^{12}–10^{13} cm^{-3} (and this corresponds to more than 10^6 cm^{-3} of OH (see **Figure 4a**)). We

9   also considered the CO abundance because OH density also depends on CO density. The

10   observed minimum abundance of CO determined by the MEX/PFS was about 400 ppm

11   (Sindoni et al., 2011), which corresponds to about 5×10^{13} cm^{-3} near the surface. We adopted

12   the minimum CO abundance and derived the lifetime of CH_4 (dotted line in **Figure 4**).

13   Although it became slightly shorter (~30 years), it is still much longer than weeks or months.

14   $O(^1D)$ and O are the other minor candidates as CH_4 sinks in the atmosphere (Wong et al.,

15   2003). The dashed lines in **Figure 4b** represent the lifetime of CH_4 with 10 times larger

16   abundances of $O(^1D)$ and O than the values predicted by Krasnopolsky (2006). In this case,

17   the lifetime of CH_4 becomes even shorter (~10 years), but it is still longer than the expected

18   short lifetime of CH_4. We conclude that according to such a long-term averaged view, it is

19   difficult to explain the observed short lifetime of CH_4 by atmospheric oxidation processes.

Our result suggests the presence of strong CH_4 sinks not subject to atmospheric oxidation, e.g., an oxidant on the surface (Atreya et al., 2007) or wind eroded grains (Jansen et al., 2014).

5. Summary

We reported on the first attempt to search for H_2O_2 in the Martian atmosphere from long-term measurements by a spacecraft-borne instrument using relatively high-dispersion spectroscopic observations with MEX/PFS. We used the strongest ν_4 band of H_2O_2 around 362 cm^{-1} and 379 cm^{-1}. Although we performed sensitive data calibrations and averaged a large number of spectra in order to search for the tiny absorptions of H_2O_2, the derived mixing ratios of H_2O_2 were close to the detection limits or upper limit. The derived mixing ratios were 16 ± 19 ppb (i.e., 35 ppb upper limit) at $Ls = 0$–$120°$, 35 ± 32 ppb at $Ls = 120$–$240°$, and 41 ± 28 ppb at $Ls = 240$–$360°$. These results restrict the oxidizing capacity in the Martian atmosphere. Regarding the issue of CH_4 sinks on Mars, we conclude that atmospheric oxidation alone cannot explain the observed short lifetime of CH_4.

6

7   **References**

8   Atreya, S.K., Mahaffy, P.R., Wong, A., 2007. Methane and related trace species on Mars:

9   Origin, loss, implications for life, and habitability. Planet. Space Sci. 55, 358–369.

10   Clancy, R.T., Sandor, B.J., Moriarty-Schieven, G.H., 2004. A measurement of the 362 GHz

11   absorption line of Mars atmospheric H_2O_2. Icarus 168, 116–121.

12   Drayson, S.R., 1976. Rapid computation of the Voight profile. J. Quant. Spectrosc. Radiat.

13   Transfer 16, 611–614.

14   Encrenaz, T., Greathouse, T.K., Bezard, B., Atreya, S.K., Wong, A.S., Richter, M.J., Lacy,

15   J.H., 2002. A stringent upper limit of the H_2O_2 abundance in the Martian atmosphere.

16   Astron. Astrophys. 396, 1037–1044.

17   Encrenaz, T., Bézard, B., Greathouse, T.K., Richter, M.J., Lacy, J.H., Atreya, S.K., Wong,

18   A.S., Lebonnois, S., Lefèvre, F., Forget, F., 2004. Hydrogen peroxide on Mars: evidence

19   for spatial and seasonal variations. Icarus 170, 424–429.

1   Encrenaz, T., Greathouse, T.K., Richter, M.J., Bézard, B., Fouchet, T., Lefèvre, F.,

2   Montmessin, F., Forget, F., Lebonnois, S., Atreya, S.K., 2008. Simultaneous mapping of

3   H_2O and H_2O_2 on Mars from infrared high-resolution imaging spectroscopy. Icarus 195,

4   547–556.

5   Encrenaz, T., Greathouse, T.K., Lefèvre, F., Atreya, S.K., 2012. Hydrogen peroxide on Mars:

6   Observations, intepretation and future plans. Planet. Space Sci. 68, 3–17.

7   Fonti, S., Marzo, G.A., 2010. Mapping of methane on Mars. Astron. Astrophys. 512, A51.

8   Forman, M.L., Steel, W.H., Vanasse, G.A., 1966. Correction of asymmetric interferograms

9   obtained in Fourier spectroscopy. J. Opt. Soc. Amer. 56 (1), 59–61.

10   Formisano, V., Atreya, S.K., Encrenaz, T., Ignatiev, N., Giuranna, M., 2004. Detection of

11   methane in the atmosphere of Mars. Science 306, 1758–1761.

12   Formisano, V., Angrilli, F., Arnold, G., Atreya, S., Bianchini, G., Biondi, D., Blanco, A.,

13   Blecka, M.I., Coradini, A., Colangeli, L., Ekonomov, A., Esposito, F., Fonti, S., Giuranna,

14   M., Grassi, D., Gnedykh, V., Grigoriev, A., Hansen, G., Hirsh, H., Khatuntsev, I., Kiselev,

15   A., Ignatiev, N., Jurewicz, A., Lellouch, E., Lopez Moreno, J., Marten, A., Mattana, A.,

16   Maturilli, A., Mencarelli, E., Michalska, M., Moroz, V., Moshkin, B., Nespoli, F.,

17   Nikolsky, Y., Orfei, R., Orleanski, P., Orofino, V., Palomba, E., Patsaev, D., Piccioni, G.,

18   Rataj, M., Rodrigo, R., Rodriguez, J., Rossi, M., Saggin, B., Titov, D., Zasova, L., 2005.

19   The Planetary Fourier Spectrometer (PFS) onboard the European Mars Express mission.

Planet. Space Sci. 53 (10), 963–974.

Fouchet, T., Lellouch, E., Ignatiev, N.I., Forget, F., Titov, D.V., Tschimmel, M., Montmessin, F., Formisano, V., Giuranna, M., Maturilli, A., Encrenaz, T., 2007. Martian water vapor: Mars Express PFS/LW observations. Icarus 190, 32–49.

Geminale, A., Formisano, V., Sindoni, G., 2011. Mapping methane in Martian atmosphere with PFS-MEX data. Planet. Space Sci. 59, 137–148.

Giuranna, M., Formisano, V., Biondi, D., Ekonomov, A., Fonti, S., Grassi, D., Hirsch, H., Khatuntsev, I., Ignatiev, N., Michalska, M., Mattana, A., Maturilli, A., Mencarelli, E., Nespoli, F., Orfei, R., Orleanski, P., Piccioni, G., Rataj, M., Saggin, B., Zasova, L., 2005a. Calibration of the Planetary Fourier Spectrometer long wavelength channel. Planet. Space Sci. 53 (10), 993–1007.

Giuranna, M., Formisano, V., Biondi, D., Ekonomov, A., Fonti, S., Grassi, D., Hirsch, H., Khatuntsev, I., Ignatiev, N., Michalska, M., Mattana, A., Maturilli, A., Moshkin, B.E., Mencarelli, E., Nespoli, F., Orfei, R., Orleanski, P., Piccioni, G., Rataj, M., Saggin, B., Zasova, L., 2005b. Calibration of the Planetary Fourier Spectrometer short wavelength channel. Planet. Space Sci. 53 (10), 975–991.

Hanel, R.A., Conrath, B.J., Jennings, D.E., Samuelson, R.E., 2003. Exploration of the Solar System by Infrared Remote Sensing, second edition, Cambridge University Press, U.K.

Hartogh, P., Jarchow, C., Lellouch, E., de Val-Borro, M., Rengel, M., Moreno, R., Medvedev, A.S., Sagawa, H., Swinyard, B.M., Cavalié, T., Lis, D.C., Błęcka, M.I., Banaszkiewicz, M., Bockelée-Morvan, D., Crovisier, J., Encrenaz, T., Küppers, M., Lara, L.-M., Szutowicz, S., Vandenbussche, B., Bensch, F., Bergin, E.A., Billebaud, F., Biver, N., Blake, G.A., Blommaert, J.A.D.L., Cernicharo, J., Decin, L., Encrenaz, P., Feuchtgruber, H., Fulton, T., de Graauw, T., Jehin, E., Kidger, M., Lorente, R., Naylor, D.A., Portyankina, G., Sánchez-Portal, M., Schieder, R., Sidher, S., Thomas, N., Verdugo, E., Waelkens, C., Whyborn, N., Teyssier, D., Helmich, F., Roelfsema, P., Stutzki, J., LeDuc, H.G., Stern, J.A., 2010. Herschel/HIFI observations of Mars: First detection of O_2 at submillimetre wavelengths and upper limits on HCl and H_2O_2. Astron. Astrophys. 521, L49.

Jansen, S.J.K., Skibsted, J., Jakobsen, H.J., Kate, I.L.T., Gunnlaugsson, H.P., Merrison, J.P., Finster, K., Bak, E., Iversen, J.J., Kondrup, J.C., Nørnberg, P., 2014. A sink of methane on Mars? The answer is blowing in the wind. Icarus 236, 24–27.

Kong, T.Y., McElroy, M.B., 1977. Photochemistry of the Martian atmosphere. Icarus 32, 168–189.

Krasnopolsky, V.A., Bjoraker, G.L., Mumma, M.J., Jennings, D.E., 1997. High-resolution spectroscopy of Mars at 3.7 and 8 μm: A sensitive search of H_2O_2, H_2CO, HCl, and CH_4, and detection of HDO. J. Geophys. Res. 102, 6525–6534.

1   Krasnopolsky, V.A., 2006. Photochemistry of the Martian atmosphere: Seasonal, latitudinal,

2   and diurnal variations. Icarus 185, 153-170.

3   Lefèvre, F., Forget, F., 2009. Observed variations of methane on Mars unexplained by known

4   atmospheric chemistry and physics. Nature 460 (7256), 720–723.

5   Mumma, M.J., Villanueva, G.L., Novak, R.E., Hewagama, T., Bonev, B.P., DiSanti, M.A.,

6   Mandell, A.M., Smith, M.D., 2009. Strong release of methane on Mars in northern

7   summer 2003. Science 323 (5917), 1041–1045.

8   Nair, H., Allen, M., Anbar, A.D., Yung, Y.L., Clancy, R.T., 1994. A photochemical model of

9   the Martian atmosphere. Icarus 111, 124–150.

10   Rothman, L.S., Rinsland, C.P., Goldman, A., Massie, S.T., Edwards, D.P., Flaud, J.-M., Perrin,

11   A., Camy-Peyret, C., Dana, V., Mandin, J.-Y., Schroeder, J., McCann, A., Gamache, R.R.,

12   Wattson, R.B., Yoshino, K., Chance, K.V., Jucks, K.W., Brown, L.R., Nemtchinov, V.,

13   Varanasi, P., 1998. The HITRAN molecular spectroscopic database and HAWKS

14   (HITRAN Atmospheric Workstation): 1996 Edition. J. Quant. Spectrosc. Radiat. Transfer

15   60, 665–710.

16   Rothman, L.S., Gordon, I.E., Barbe, A., Chris Benner, D., Bernath, P.F., Birk, M., Boudon, V.,

17   Brown, L.R., Campargue, A., Champion, J.-P., Chance, K., Coudert, L.H., Dana, V., Devi,

18   V.M., Fally, S., Flaud, J.-M., Gamache, R.R., Goldman, A., Jacquemart, D., Kleiner, I.,

19   Lacome, N., Lafferty, W.J., Mandin, J.-Y., Massie, S.T., Mikhailenko, S.N., Miller, C.E.,

1   Moazzen-Ahmadi, N., Naumenko, O.V., Nikitin, A.V., Orphal, J., Perevalov, V.I., Perrin,

2   A., Predoi-Cross, A., Rinsland, C.P., Rotger, M., Simeckova, M., Smith, M.A.H., Sung, K.,

3   Tashkun, S.A., Tennyson, J., Toth, R.A., Vandaele, A.C., Vander Auwera, J., 2009. The

4   HITRAN 2008 molecular spectroscopic database. J. Quant. Spectrosc. Radiat. Transfer

5   110, 533–572.

6   Saggin, B., Scaccabarozzi, D., Tarabini, M., 2011. Instrumental phase-based method for

7   Fourier transform spectrometer measurements processing. Appl. Opt. 50, 1717–1725.

8   Sander, S.P., Golden, D.M., Kurylo, M.J., Moortgat, G.K., Wine, P.H., Ravishankara, A.R.,

9   Kolb, C.E., Molina, M.J., Finlayson-Pitts, B.J., Huie, R.E., Orkin, V.L., 2006. Chemical

10   kinetics and photochemical data for use in atmospheric studies evaluation number 15. JPL

11   Publ. 06-3, Jet Propul. Lab., Pasadena, Calif.

12   Sindoni, G., Formisano, V., Geminale, A., 2011. Observations of water vapour and carbon

13   monoxide in the Martian atmosphere with the SWC of PFS/MEX. Planet. Space Sci. 59,

14   149–162.

15   Smith, M.D., Bandfield, J.L., Christensen, P.R., 2000. Separation of atmospheric and surface

16   spectral features in Mars Global Surveyor Thermal Emission Spectrometer (TES) spectra.

17   J. Geophys. Res. 105 (E4), 9589–9607.

18   Smith, M.D., 2002. The annual cycle of water vapor on Mars as observed by the Thermal

19   Emission Spectrometer. J. Geophys. Res. 107, E11.

1   Villanueva, G.L., Mumma, M.J., Bonev, B.P., Noval, R.E., Barber, R.J., Disanti, M.A., 2012.

2   Water in planetary and cometary atmospheres: H_2O/HDO transmittance and fluorescence

3   models. J. Quant. Spectrosc. Radiat. Transfer 113, 202–220.

4   Wong, A.S., Atreya, S.K., Encrenaz, T., 2003. Chemical markers of possible hot spots on

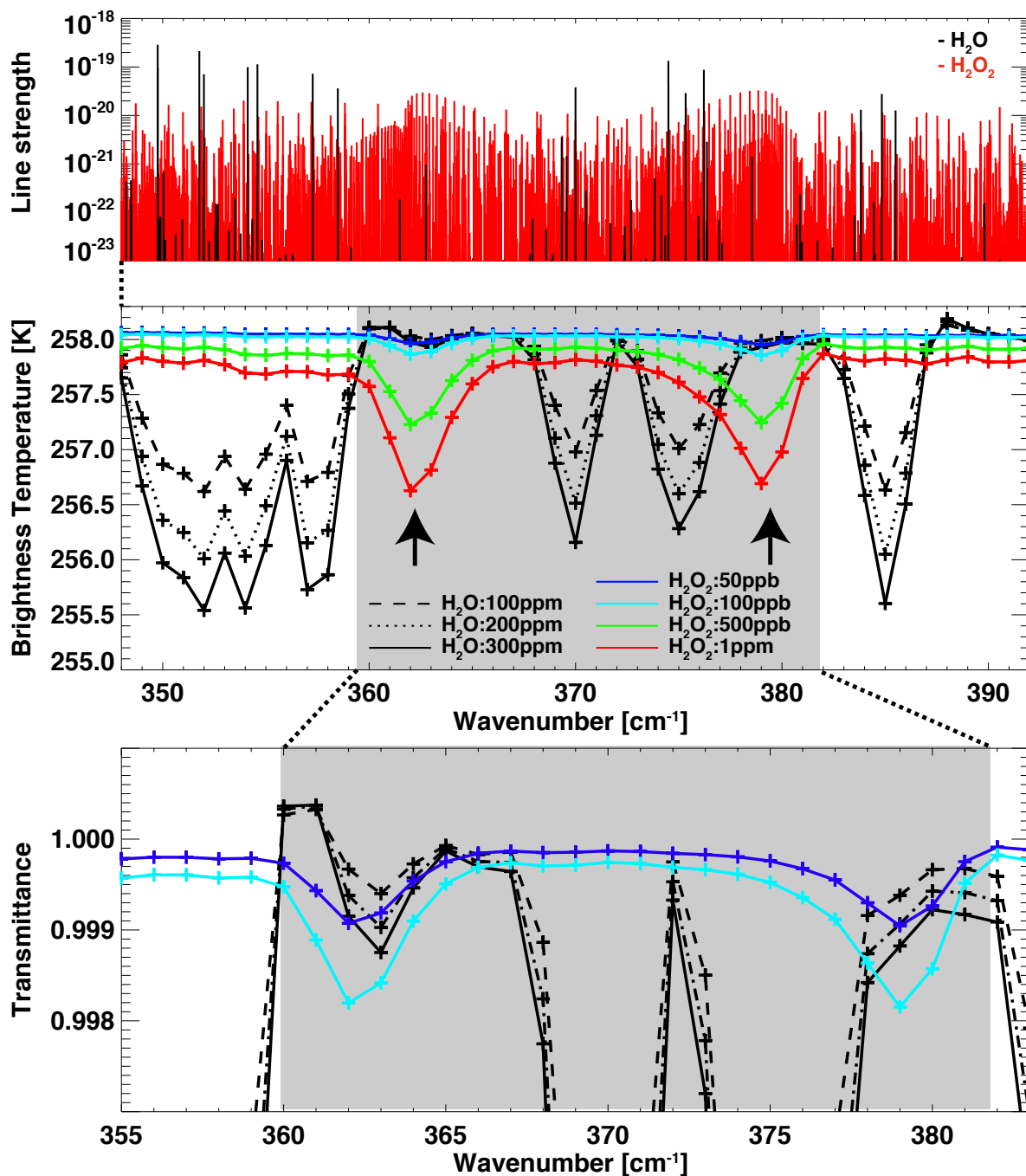5   Mars. J. Geophys. Res. 108 (E4), 5026.

6

7

8

9

10

11

12

13

14

15

16

17

18

19

3   **Figure 1.** (Top) Line strength of H_2O and H_2O_2 in the spectral range between 350 and 390

4   cm^{-1} obtained from HITRAN08. (Middle) Synthetic spectra in the spectral range between 350

5   and 390 cm^{-1} with the spectral resolution of the apodized PFS spectrum. The black curves

6   show the spectra with various mixing ratios of H_2O (dash: 100 ppm, dot: 200 ppm, solid: 300

7   ppm). The color curves show the spectra with various mixing ratios of H_2O_2 (blue: 50 ppb,

1   light blue: 100 ppb, green: 500 ppb, red: 1 ppm). The arrows show the spectral features used

2   for the search of H_2O_2. The gray box represents the spectral ranges used in this analysis as

3   shown in **Figure 3**. (Bottom) The same as in the middle figure but with a different Y-axis

4   scale. Note that an enhanced feature around 361 cm^{-1} in the spectra of H_2O is due to the

5   side-lobes in the instrumental line shape of the PFS (Giuranna et al., 2005b).
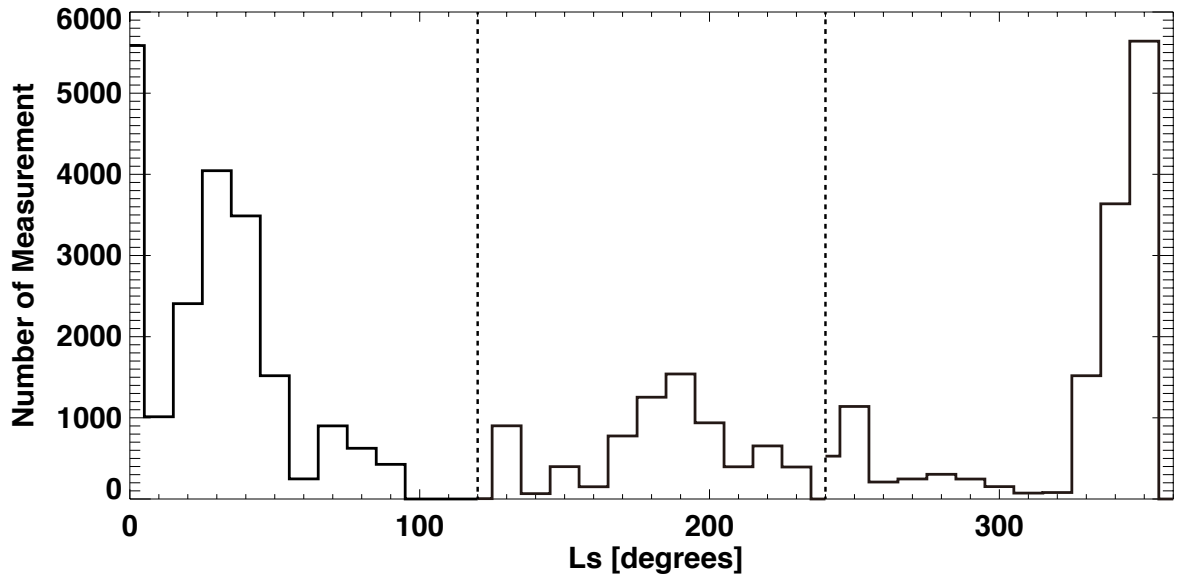
6

7

8

9

10

11

12

13

14

15

16

17

18

19

1

2   **Figure 2.** The distributions of solar longitude L_s in the three datasets that were used. The

3   histogram shows the numbers of measurements as a function of the solar longitude. The

4   interval of the histogram is 10°.

5

6

7

8

9

10

11

12

13

14

(a) Ls: 0-120

Legend (top panel):
- PFS data
- Best-Fit (16 ppb)
- H_2O_2: 0 ppb
- H_2O_2: 20 ppb
- H_2O_2: 40 ppb
- H_2O_2: 60 ppb
- H_2O_2: 100 ppb

Top panel axis: Brightness Temperature [K]

H_2O_2 H_2O H_2O H_2O_2

Legend (bottom panel):
- (PFS data) − (H_2O_2: 0ppb)
- (Best-Fit) − (H_2O_2: 0ppb)
- (H_2O_2: 20ppb) − (H_2O_2: 0ppb)
- (H_2O_2: 40ppb) − (H_2O_2: 0ppb)
- (H_2O_2: 60ppb) − (H_2O_2: 0ppb)
- (H_2O_2: 100ppb) − (H_2O_2: 0ppb)

H_2O_2 (ppb) = 16 ± 19
H_2O (cm^{-2}) = 2.43x10^{19}

Bottom panel axis: Residuals [erg/sr/cm²/cm^{-1}]

Wavenumber [cm^{-1}]

1

(b) Ls: 120-240

Upper panel — Brightness Temperature [K] vs Wavenumber [cm⁻¹]:

- H$_2$O$_2$
- H$_2$O
- H$_2$O
- H$_2$O$_2$

Legend:
- PFS data
- Best-Fit (35 ppb)
- H$_2$O$_2$:   0 ppb
- H$_2$O$_2$: 20 ppb
- H$_2$O$_2$: 40 ppb
- H$_2$O$_2$: 60 ppb
- H$_2$O$_2$: 100 ppb

Lower panel — Residuals [erg/sr/cm²/cm⁻¹] vs Wavenumber [cm⁻¹]:

Legend:
- (PFS data)   - (H$_2$O$_2$: 0ppb)
- (Best-Fit)   - (H$_2$O$_2$: 0ppb)
- (H$_2$O$_2$: 20ppb) - (H$_2$O$_2$: 0ppb)
- (H$_2$O$_2$: 40ppb) - (H$_2$O$_2$: 0ppb)
- (H$_2$O$_2$: 60ppb) - (H$_2$O$_2$: 0ppb)
- (H$_2$O$_2$: 100ppb) - (H$_2$O$_2$: 0ppb)

H$_2$O$_2$ (ppb) = 35 ± 32
H$_2$O (cm^{-2}) = 3.52x10^{19}

1

Figure 3. The PFS averaged spectra over (a) *Ls* = 0–120°, (b) *Ls* = 120–240°, and (c) *Ls* =

240–360° in the spectral range between 359 and 382 cm^{-1}. (Top) Comparison between the

synthetic spectra and the averaged PFS spectra. The red curves show the best-fit synthetic

spectra. The other color curves represent synthetic spectra with various mixing ratios of H_2O_2

(blue: 20 ppb, light blue: 40 ppb, green: 60 ppb, orange: 100 ppb). The black vertical bars

show instrumental noise calculated by the noise equivalent radiance divided by the square root

of the number of measurements. (Bottom) Residual spectra, where special synthetic spectra

with all contributions except H_2O_2 have been subtracted from the measured and synthetic

(including H_2O_2 contribution) spectra. The retrieved H_2O_2 values are 16 ± 19 ppb at *Ls* =

1   0–120° (i.e., 35 ppb upper limit), 35 ± 32 ppb at Ls = 120–240°, and 41 ± 28 ppb at Ls =

2   240–360°; the derived H_2O column densities in the three averages were 2.43×10^{19} cm^{-2}, 3.52

3    $\times 10^{19}$ cm^{-2}, and 2.50×10^{19} cm^{-2}, respectively. The red vertical bars show instrumental noise

4   estimated from the standard deviation of the residuals between the PFS data and the best-fit

5   synthetic spectra.

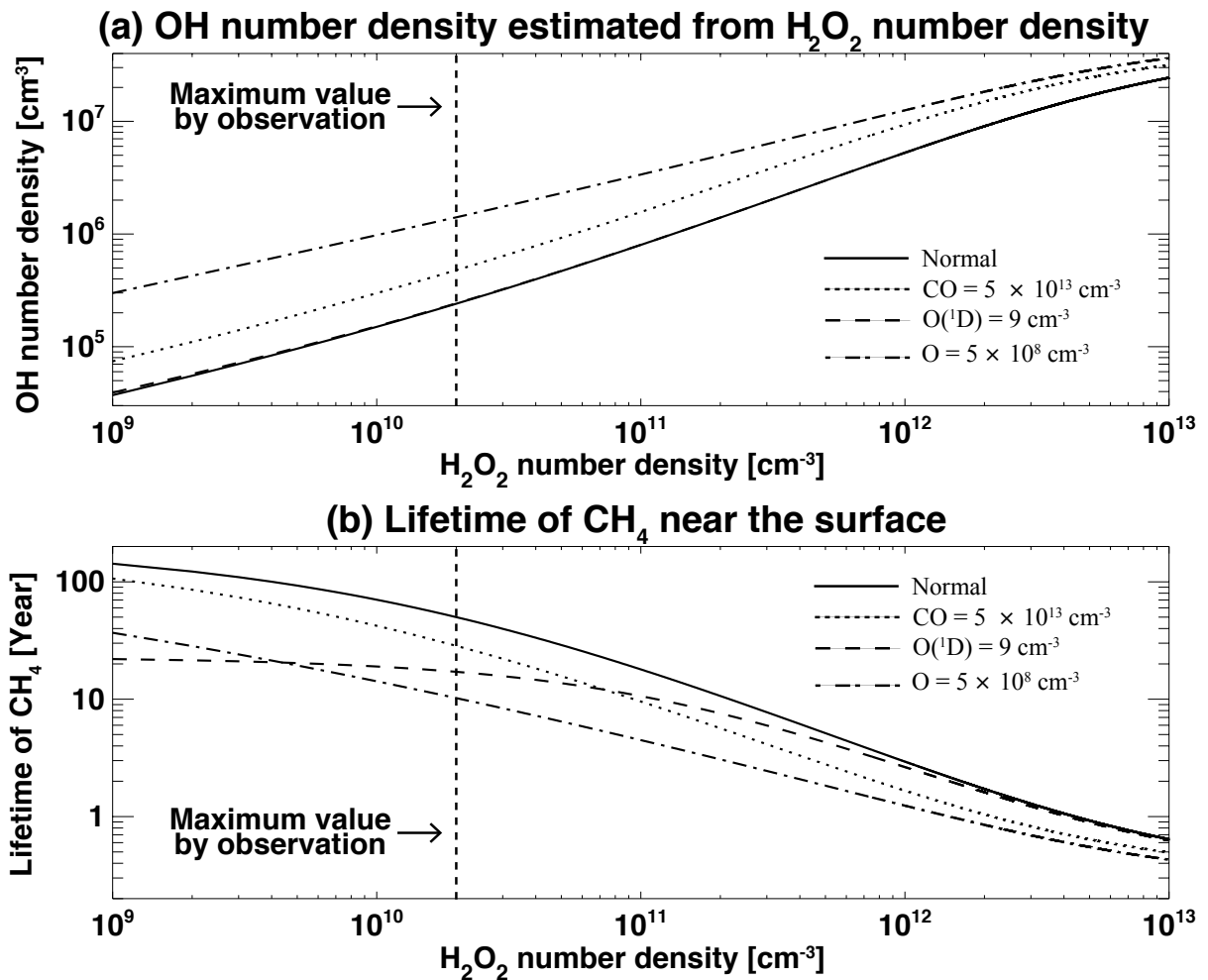6

7

8

9

10

11

12

13

14

15

16

17

18

19

(a) OH number density estimated from H_2O_2 number density

(b) Lifetime of CH_4 near the surface

1

2   **Figure 4.** (a) OH number density estimated from the H_2O_2 number density. (b) Estimated

3   photochemical lifetime of CH_4 with the abundances of H_2O_2 near the surface. Our

4   observations showed that the maximum mixing ratio of H_2O_2 is 1.1×10^{10} cm^{-3} near the

5   surface. The solid line represents the lifetime with the normal input parameters listed in **Table**

6   **2**. The dotted line represents the lifetime with rich CO conditions (5×10^8 cm^{-3}). The dashed

7   lines represent the lifetime with rich O(^{1}D) and O conditions, and these were 10 times larger

8   than the values predicted in Krasnopolsky et al. (2006).

9